THE OFFICIAL MAGAZINE OF THE OCEANOGRAPHY SOCIETY

Oceanography

CITATION

Estournel, C., P. Testor, I. Taupier-Letage, M.-N. Bouin, L. Coppola, P. Durand, P. Conan, A. Bosse, P.-E. Brilouet, L. Beguery, S. Belamari, K. Béranger, J. Beuvier, D. Bourras, G. Canut, A. Doerenbecher, X. Durrieu de Madron, F. D'Ortenzio, P. Drobinski, V. Ducrocq, N. Fourrié, H. Giordani, L. Houpert, L. Labatut, C.L. Brossier, M. Nuret, L. Prieur, O. Roussot, L. Seyfried, and S. Somot. 2016. HyMeX-SOP2: The field campaign dedicated to dense water formation in the northwestern Mediterranean. *Oceanography* 29(4):196–206, https://doi.org/10.5670/oceanog.2016.94.

DOI

https://doi.org/10.5670/oceanog.2016.94

HyMeX-SOP2

The Field Campaign Dedicated to Dense Water Formation in the Northwestern Mediterranean





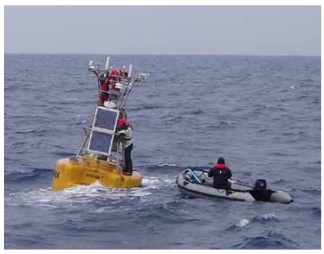

By Claude Estournel, Pierre Testor, Isabelle Taupier-Letage, Marie-Noelle Bouin, Laurent Coppola, Pierre Durand, Pascal Conan, Anthony Bosse, Pierre-Etienne Brilouet, Laurent Beguery, Sophie Belamari, Karine Béranger, Jonathan Beuvier, Denis Bourras, Guylaine Canut, Alexis Doerenbecher, Xavier Durrieu de Madron, Fabrizio D'Ortenzio, Philippe Drobinski, Véronique Ducrocq, Nadia Fourrié, Hervé Giordani, Loïc Houpert, Laurent Labatut, Cindy Lebeaupin Brossier, Mathieu Nuret, Louis Prieur, Odile Roussot, Leo Seyfried, and Samuel Somot

ABSTRACT. The HYdrological cycle in the Mediterranean Experiment (HyMeX) Special Observing Period 2 (SOP2, January 27–March 15, 2013) was dedicated to the study of dense water formation in the Gulf of Lion in the northwestern Mediterranean. This paper outlines the deep convection of winter 2012–2013 and the meteorological conditions that produced it. Alternating phases of mixing and restratification are related to periods of high and low heat losses, respectively. High-resolution, realistic, three-dimensional models are essential for assessing the intricacy of buoyancy fluxes, horizontal advection, and convective processes. At the submesoscale, vertical velocities resulting from symmetric instabilities of the density front bounding the convection zone are crucial for ventilating the deep ocean. Finally, concomitant atmospheric and oceanic data extracted from the comprehensive SOP2 data set highlight the rapid, coupled evolution of oceanic and atmospheric boundary layer characteristics during a strong wind event.

INTRODUCTION

Observations of oceanic convection leading to dense water formation (DWF) have been collected in a variety of regions, including the Greenland, Labrador, Mediterranean, and Weddell Seas (see Marshall and Schott, 1999, for a review). The formation of dense water happens in three phases. First, water is preconditioned due to basin-scale doming of isopycnals. Second, convective plumes (characterized by high down- and upward vertical velocities) develop, and a mixed patch forms, with associated eddy activity within it and on its edge. Third, in the phase termed "spreading," water and buoyancy from the mixed patch are exchanged with the surrounding stratified waters, with baroclinic instability a key mechanism orchestrating the exchange (MEDOC group, 1970). Although these phases are described separately, questions remain about whether and how they overlap as a result of the intermittent nature of atmospheric forcing, which drives the convection (Houpert et al., 2016). Indeed, dynamical processes in both the atmosphere and the ocean act on similar time scales during periods of oceanic convection: strong wind events related to high heat and freshwater exchanges between the ocean and the atmosphere have a typical duration of a few days. The water column can mix over the same time scale. At spatial scales, there is no significant difference between the convective and the baroclinic eddy scales (Marshall and Schott, 1999). Marshall and Schott (1999, p. 36) emphasize the "fascinating and central aspect of the convective process in the ocean, which is the interaction between convection and baroclinic instability." If buoyancy is extracted rapidly through violent events, baroclinic instability does not have enough time to limit the convection depth, whereas in the case of lower cooling rates, baroclinic instability may indeed control the depth reached by the mixed layer (Visbeck et al., 1996). This is probably a major reason why no relationship has been proven between the volume of water formed, its hydrological characteristics, and atmospheric forcing (e.g., the heat and water losses integrated over winter).

Study of the interaction between horizontal and vertical processes under realistic conditions is itself complex because of (1) the need for data that describe the variability of convection at small spatial scales (a few kilometers) and at high frequency (typically a day), (2) the difficulty of making accurate concomitant observations throughout the water column and the atmosphere during wintertime, and (3) uncertainties (especially for strong wind events) in the bulk formulae used to calculate air-sea fluxes and the frequent underestimation of very strong winds by atmospheric models (Hauser et al., 2003). The latter is a major sticking point for ocean models. Moreover, it is known that the eddy-permitting models used for climate studies overestimate DWF compared to eddy-resolving ones (Herrmann et al., 2008), as the exchanges between the mixed patch and the stratified waters are reduced by the lack of mesoscale eddies. Thus, there is a need for parameterizations to avoid drift in climatic simulations.

The HYdrological cycle in the Mediterranean Experiment (HyMeX, 2010–2020; Drobinski et al., 2014) fosters synergy among different scientific communities in order to monitor and model the Mediterranean atmosphere-land-ocean coupled system, its variability, and its long-term evolution. The first HyMeX Special Operating Period, SOP1 (September 15–November 15, 2012), was dedicated to gathering data on high-precipitation events and flash floods (Ducrocq et al., 2014). The objectives of SOP2 (January 27–March 15, 2013), the focus of this article, were (1) to acquire a data set sufficiently extensive in space and time to study the processes governing dense water formation and spreading in the Gulf of Lion (northwestern Mediterranean) and their interactions at the scale of meteorological events, and (2) to test the ability of ocean models at different horizontal resolutions to reproduce the characteristics of the newly formed dense water. The Mediterranean basin is particularly suitable for DWF studies because the water column has been monitored over the long term, providing an extended time frame perspective to this short-term experiment; the spatial scales involved are smaller there than in the open ocean; and atmospheric

Photos from opposite page. (background) View of R/V *Le Suroît* and the Gulf of Rosas during the DEep Water formation Experiment (DEWEX) cruise. *Credit: Pierre Testor* From left to right: (1) CTD rosette. *Credit: Laurent Coppola* (2) Autonomous gliders. *Credit: Pierre Testor* (3) Waverider deployment from R/V *Tethys II*. *Credit: Isabelle Taupier-Letage* (4) Retrieving a glider during the DEWEX cruise. *Credit: Xavier Durrieu de Madron* (5) Servicing the Lion meteorological buoy. *Credit: Isabelle Taupier-Letage*

and sea state conditions are somewhat milder than in polar regions, facilitating the deployment of instruments at sea.

This article first describes the HyMeX-SOP2 general setup, which was designed to span the temporal and spatial scales of the processes involved in DWF. Next, we discuss the meteorological and convection characteristics of winter 2012–2013, and the succession of mixed and stratified vertical density profiles is compared with the intermittent atmospheric forcing. The role that vertical and horizontal processes, including those at the submesoscale, play in convection is then discussed. Finally, we present atmosphere and ocean data collected during a late convection event. Our description of the very large data sets collected is intended to inspire scientists to join a similar experiment in the eastern basin of the Mediterranean, which is expected in a few years.

GULF OF LION

Convection in the Gulf of Lion is induced by high levels of cooling and evaporation due to the prevailing cold, dry, northerly local winds (Mistral and Tramontane; Figure 1a), along with cyclonic circulation associated with the doming of isopycnals, which facilitates mixing with the saltier underlying waters. During winter, the cyclonic circulation is reinforced, isolating water in the gulf's central part and favoring heat loss. Importantly, convection in the Gulf of Lion exhibits interannual variability, both in time (years with or without DWF) and in space: the vertical extent of the convection varies between a few hundred meters and the whole water column (~2,500 m; Mertens and Schott, 1998; Somot et al., 2016), and its horizontal extent from a few tens of kilometers to ~100 km. This convection feeds thermohaline circulation through the transformation of waters of Atlantic origin into intermediate and deep water masses, called Winter Intermediate Water and Western Mediterranean Deep Water, respectively. During the spreading phase, about 50% of the newly formed dense water is incorporated into the Northern Current (see Figure 1a for location), and 50% is transported great distances by numerous, long-lived anticyclonic and cyclonic eddies (Send et al., 1996; Testor and Gascard, 2006; Bosse et al., 2016).

EXPERIMENTAL DESIGN AT VARIOUS TEMPORAL SCALES

Following the HyMeX observation strategy, monitoring of the northwestern Mediterranean was organized at three different temporal scales: interannual, annual, and seasonal. Monitoring at the interannual scale (Long Observation Period) was achieved by the MOOSE (Mediterranean Ocean Observing System for the Environment; http://www.moose-network.fr) integrated observing system, whose aim was to observe the impact of climate on the evolution of the hydrology and biogeochemistry of the northwestern Mediterranean. Annual-scale monitoring (Enhanced Observation Period) benefited from the synergy of several programs—MOOSE, MERMEX (Marine Ecosystems Response in the Mediterranean Experiment), and HyMeX SOP1—and included collecting data on water column stratification, in particular in summer, in order to assess the dense water budget (difference of volume and changes in density before and after winter). Stratification data are also

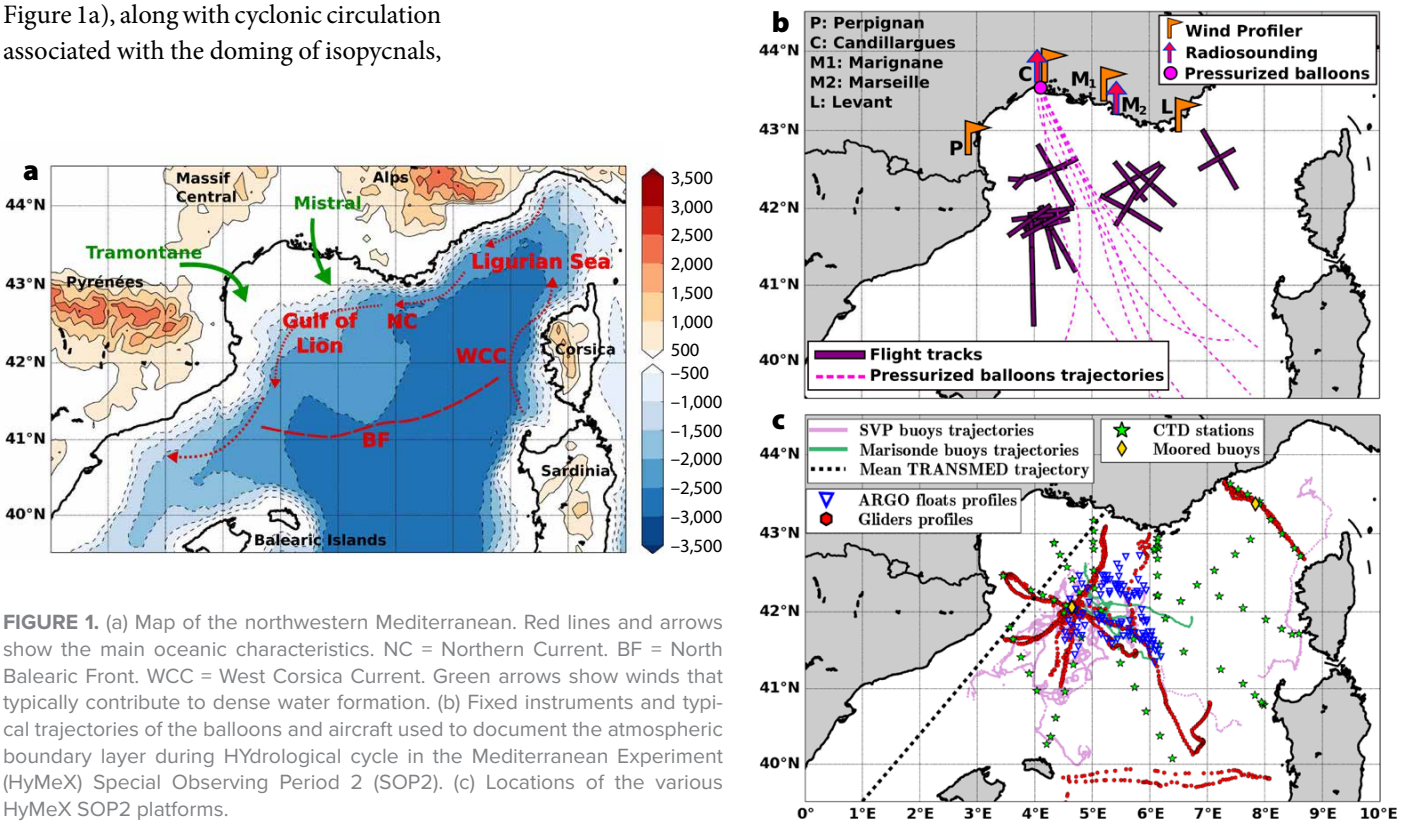

FIGURE 1. (a) Map of the northwestern Mediterranean. Red lines and arrows show the main oceanic characteristics. NC = Northern Current. BF = North Balearic Front. WCC = West Corsica Current. Green arrows show winds that typically contribute to dense water formation. (b) Fixed instruments and typical trajectories of the balloons and aircraft used to document the atmospheric boundary layer during HYdrological cycle in the Mediterranean Experiment (HyMeX) Special Observing Period 2 (SOP2). (c) Locations of the various HyMeX SOP2 platforms.

important for understanding the central role autumn plays in the seasonal cycle, corresponding to the preconditioning phase and the first deepening of the mixed layer. SOP2 focused on the seasonal scale, using an existing but enhanced monitoring network as well as specific deployments that targeted the most interesting events in order to understand how the oceanic mixed layer deepens through convective processes. Figure 1b,c shows the locations of the instruments used to monitor the ocean and the atmosphere at the different temporal scales.

Long-term and Enhanced Observation Periods

Sensors on two Météo-France buoys known as Lion in the Gulf of Lion and Azur in the Ligurian Sea measure the parameters needed to calculate the heat and water budgets (i.e., atmospheric parameters, radiative fluxes, and sea surface temperature). An omnidirectional Waverider on each buoy collects wave spectrum data. Each of these buoys is also equipped with 20 temperatures sensors that span the upper 250 m of the water column, as well as a surface salinity sensor. These measurements complement the vertical temperature and salinity profiles acquired at 21 temperature and 15 salinity levels between 150 m and 2,300 m water depth on the LION mooring line (different from the Lion buoy), supported by MOOSE, that have been available since 2007.

Thanks to MOOSE and the European PERSEUS (Policy-oriented marine Environmental Research for the Southern European Seas) program, numerous glider deployments (13 in 2012) were conducted in the Ligurian Sea and in the Gulf of Lion. The gliders measured depth-averaged currents, temperature, salinity, and dissolved oxygen, as well as other biogeochemical variables such as chlorophyll-*a* fluorescence and turbidity.

A ship of opportunity, *Marfret-Niolon*, during weekly crossings between Marseille and Algeria, provided information on north-south, cross-basin variability of air-sea characteristics by continuously recording sea surface temperature (SST), sea surface salinity (SSS), and meteorological parameters (wind, temperature, and humidity).

At the regional scale, MOOSE conducts summer surveys of the stratification of the water masses in the Gulf of Lion and the Ligurian Sea. In August 2012 and in June 2013, 80 to 90 CTD casts were performed. In September 2012, February 2013, April 2013, and September 2013, MERMEX organized cruises to acquire CTD data at the same locations as MOOSE (Waldman et al., 2016). Data from the August 2012 cruise were used to provide the initial stratification in regional circulation models, and these data have proven to be crucial for precise DWF modeling (Estournel et al., 2016).

Special Observation Period 2

HyMeX SOP2 documented the DWF zones of the northwestern Mediterranean, mainly in the Gulf of Lion and, to a lesser extent, in the Ligurian Sea, where dense waters rarely form. Collecting in situ measurements during strong wind events is always challenging—winds above 25 m s^{-1} and waves as high as 7 m ($H_{1/3}$) were recorded at the Lion buoy. Thus, the SOP2 strategy for data gathering relied strongly on the deployment of autonomous platforms that are less affected by weather and sea conditions.

Observations at the Air-Sea Interface and in the Upper Water Column

Five Marisonde drifting buoys measured near-surface atmospheric pressure, wind, and air temperature, and they were also equipped with 300 m-long thermistor chains to measure water column temperature. Seven Surface Velocity Program (SVP) drifters were deployed as well, some equipped with 80 m-long thermistor chains and others with SST and SSS sensors (Figure 1c).

Limited ship time was available on the French oceanographic research vessels *Tethys II* and *Le Suroît*, so the seagoing buoy tender *Provence* was chartered to complete collection of needed in situ observations. Direct measurements of air-sea turbulent and radiative fluxes were collected (Bourras et al., 2009) using a set of instruments installed at the top of the *Provence* bow mast. Three different methods were used to calculate the turbulent fluxes: bulk, inertial-dissipation, and eddy-covariance.

Deep Ocean Observations

In winter 2012–2013, evolution of thermohaline characteristics of the water masses was monitored at high frequency through deployment of a large number of autonomous profiling floats and gliders, as well as during dedicated research cruises. Four Argo floats equipped with oxygen sensors were added to the six existing floats in the Gulf of Lion. The floats were dedicated to documenting mixing in the deeper oceanic layers. Consequently, the type of floats used during this Special Observation Period were capable of switching from the classical MedArgo cycle of one profile over 1,000 m every five days, with a parking depth at 350 m, to a DWF cycle of one full-depth profile (2,000 m) daily with a parking depth at 1,000 m. This strategy was aimed at monitoring thermohaline changes in the water column at high frequency and at minimizing the drift of the floats to increase their presence in the convective zone.

During SOP2, up to nine gliders were deployed simultaneously to collect data from the Balearic Islands to the Ligurian Sea (Figure 1c). They documented the upper 1,000 m of the water column at high spatial resolution (profiles spaced about 4 km apart) and at high frequency (of the order of six dives per day).

Approximately 100 CTD casts were made during the 20-day DEWEX (DEep Water formation EXperiment) cruise aboard R/V *Le Suroît* organized by MERMEX (February 3–21, 2013) and during the short cruises of R/V *Tethys II* (January 29–30 and February 20–21, 2013) and the buoy tender vessel *Provence* (March 7–10, 2013).

Observations in and above the Marine Atmospheric Boundary Layer

Oceanic and marine atmospheric boundary layers interact through surface fluxes of heat, moisture, and momentum. These fluxes are dependent on air temperature, moisture, and wind and, in turn, they modify these parameters. The atmospheric boundary layer (ABL) is generally well mixed but presents noteworthy discontinuities at the interface with the upper free troposphere. The fluxes at the top of the ABL can entrain and modify the "bulk" characteristics of the ABL and hence the surface fluxes. For this reason, it was decided to document not only the surface fluxes, but also the turbulence structure of the whole ABL, up to the upper interface with the free troposphere.

French ATR42 aircraft documented the air mass during strong wind conditions by measuring fluctuations in turbulence (allowing turbulent fluxes to be computed through the eddy correlation method) as well as turbulence parameters (Canut et al., 2010). The planes usually flew at six to eight levels ranging from 150 m to about 1,200 m altitude, with flight levels adjusted based on the ABL thickness obtained from an initial vertical profile.

Fifteen pressurized balloons were launched near Montpellier airport (M1 in Figure 1b) to drift at constant density levels over the sea while sampling temperature and humidity along the path of the air mass (Doerenbecher et al., 2016). In addition, 38 radiosondes were launched, some of them at Montpellier to assist in choosing balloon flight levels, and the others at Marseille (M2 in Figure 1b) and from *Provence*. Finally, a network of five coastal UHF radars, four of them around the Gulf of Lion and one in Corsica, recorded vertical profiles of wind from 100 m to 4 km every 15 minutes.

Science and Operations Coordination

The SOP2 field campaign lasted from January 27 to March 15, 2013. During this period, there were several episodes of strong, cold winds that resulted in the progression of oceanic convection down to the seafloor.

As described for HyMeX SOP1 (Ducrocq et al., 2014), scientific staff organized science missions, intensive observation periods, and deployment of on-demand instrumented platforms based on analysis of the outputs of atmospheric and ocean forecast models and of the recent oceanic observations mostly available in near-real time.

The SOP2 experiment collected the largest number of temperature and salinity profiles during a period of deep water formation in all oceanic convection areas in the world ocean. About 100 CTD profiles are available from the surface to the seafloor, and 250 Argo profiles between 0 m and 2,000 m water depth. Glider days between January and March numbered about 350, providing about 2,000 profiles between 0 m and 1,000 m water depth.

METEOROLOGICAL CHARACTERISTICS OF WINTER 2012–2013

The winter wind regime in the Gulf of Lion is usually characterized by alternating strong northerly or northwesterly winds (Mistral and Tramontane) and moderate easterly to southerly winds associated with precipitation. Mistral and Tramontane (see Figure 1a) are orographic winds that blow continental cold, dry air over the Gulf of Lion and induce intense heat, freshwater, and momentum exchanges with the sea surface. In the following, we refer largely to the atmospheric and subsurface parameters observed at the Lion buoy, which are representative of the atmospheric conditions above the Gulf of Lion DWF area.

Figure 2 presents wind speed and direction, the difference between sea surface and air temperatures, and the difference between the saturated specific humidity over seawater and the air specific humidity measured at the Lion buoy. These quantities determine the sensible and latent heat fluxes (and thus the evaporation). A statistical analysis

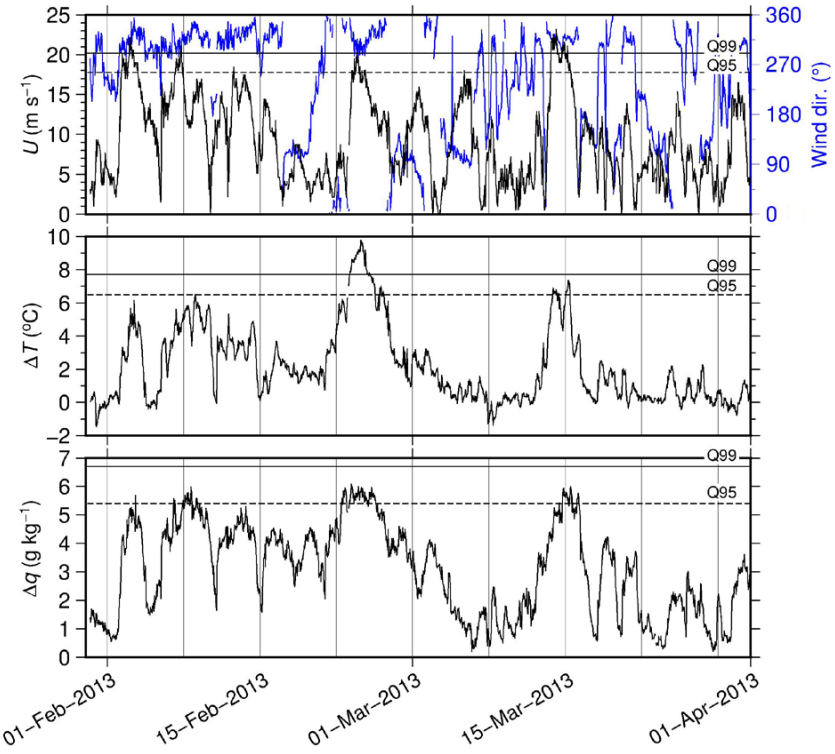

FIGURE 2. Time series of 10 m wind speed (top, black, m s^{-1}) and direction (top, blue, degrees from north), surface temperature gradient (middle, sea surface temperature minus 2 m air temperature, °C), and surface specific humidity gradient (bottom) observed at the Lion buoy during SOP2. Solid horizontal lines indicate the Q99 and dashed lines indicate Q95 limits with respect to the 2002–2011 climatology (see text).

was performed to compare the measurements for the SOP2 period to a 10-year climatology assembled based on December-to-February buoy measurements between 2002 and 2011. SOP2 values were very close to the climatology not only for the mean wind but also for the strongest winds (95th and 99th percentiles of the climatology—Q95 and Q99 in the following—were equal to 17.8 m s^{-1} and 20.2 m s^{-1}, respectively). The extreme values of temperature and specific humidity differences were clearly more frequent during winter 2012–2013 than in the climatology (temperature difference: Q95 = 6.5°C, Q99 = 7.7°C; specific humidity difference: Q95 = 5.4 g kg^{-1}, Q99=6.7 g kg^{-1}). Temperature difference exceeded Q95 during 12.2% of the period and specific humidity difference exceeded Q95 during 10.9%. The corresponding wind direction (Figure 2) was northerly to northwesterly, bringing in cold and dry air (maximum temperature difference 9.8°C, maximum specific humidity difference 5.9 g kg^{-1}). This indicates that there were stronger than average air-sea exchanges in winter 2012–2013, due to the air-sea temperature and humidity gradients rather than to wind speed.

The corresponding radiative and turbulent fluxes (Figure 3a) clearly show that the major heat and water losses are due to the latent heat flux. While the solar radiation daily maximum still reaches values higher than 400 W m^{-2} during Mistral/Tramontane events, the turbulent heat fluxes (latent, and to a lesser extent sensible, flux) can more than compensate for this heat transfer on several consecutive days, as shown by the resulting net heat flux (Figure 3b). In order to evaluate the uncertainty brought into the turbulent-flux estimates by the bulk formulation used, net heat fluxes resulting from several widely used bulk formulae are compared in Figure 3b. The COARE 3.0 algorithm (Fairall et al., 2003) is used with different formulations of surface roughness: (1) with a constant Charnock parameter (COARE), (2) using the Oost et al. (2002) formula relating surface roughness to wave age only (COARE 1), and (3) with the Taylor and Yelland (2001) formula using the peak period and the significant wave height (COARE 2). Figure 3b also plots the results from Moon et al. (2007); Ecume (Belamari and Pirani, 2007, used in the Météo-France models); and Andreas et al. (2008), which accounts for sea spray. Observed wave parameters and atmospheric and ocean surface parameters at the Lion buoy were used to process the corresponding turbulent fluxes. The mean heat loss as seen by all the algorithms is −126 ± 11 W m^{-2} during the SOP2 period and, if restricted to the wind speeds above 15 m s^{-1} (most prone to trigger DWF), 548 ± 26 W m^{-2}. The maximum difference in hourly values of the net heat flux obtained by using different algorithms is 239 W m^{-2}. Turbulent heat fluxes are also estimated from the lowest aircraft flight level, approximately 150 m above the sea surface. They corroborate tendencies based on bulk formulae even if differences are observed. Airborne measurements offer one of the only direct sources of information on heat flux, and a method for extrapolating this data down to the surface is currently being developed.

CHARACTERISTICS OF CONVECTION DURING WINTER 2012–2013

Tracking the progress of convection with mixed layer depth based on a threshold of the vertical density gradient is difficult in the Mediterranean, as these gradients are low beneath the surface layer (0 m to ~300 m). The stratification index

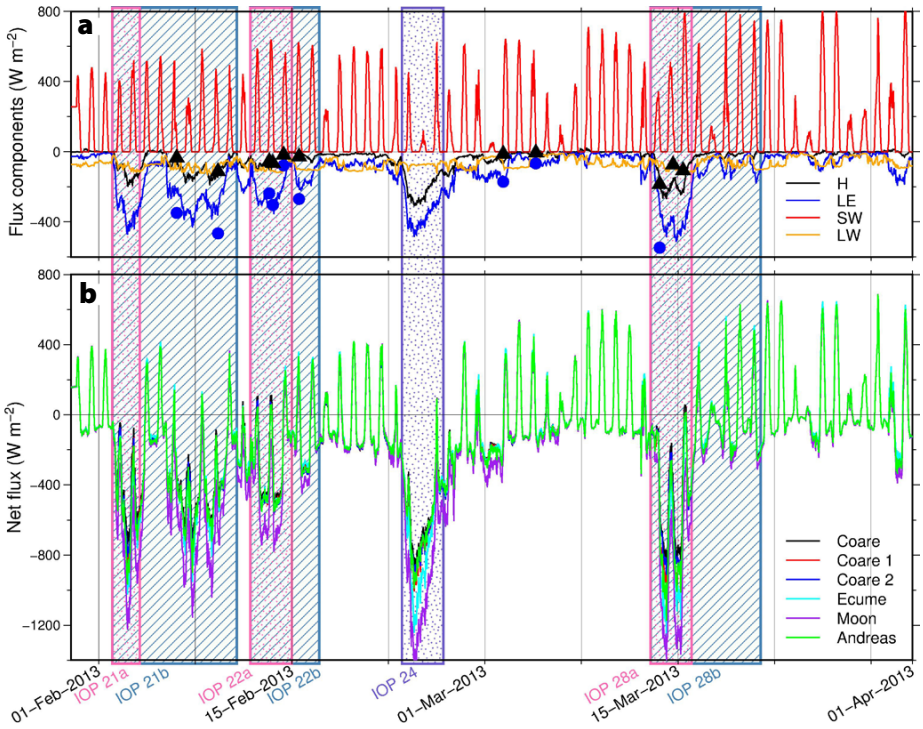

FIGURE 3. (a) Time series of radiative and turbulent fluxes measured during SOP2 (W m^{-2}). Sensible heat flux (H, black), latent heat flux (LE, blue), shortwave radiative flux (SW, red), and longwave radiative flux (LW, orange) are computed from Lion buoy observed parameters using the COARE 3.0 (Fairall et al., 2003) algorithm for the turbulent portion and the Bignami et al. (1995) formulae for the upward radiative portion. Blue circles and black triangles represent, respectively, the latent and sensible heat fluxes measured by the aircraft along its lowest flight path. (b) Time series of net heat flux (W m^{-2}) during the same period computed using different bulk formulae. The black line indicates COARE (Fairall et al., 2003) without wave impact, red is COARE 1 with wave-age effect, blue is COARE 2 with peak period and significant height effects, cyan is Ecume (Belamari and Pirani, 2007), purple is MOON (Moon et al., 2007), and green is Andreas (Andreas et al., 2008). IOPs corresponding to Mistral/Tramontane events are indicated in pink, DWF and Mistral/Tramontane events in purple, and DWF only (no strong wind) in blue.

(*SI*), which provides an objective measure of the amount of buoyancy that should be extracted to achieve the complete mixing of the water column, was then preferred:

$$SI(Z) = \int_{-z}^{0} \left(\rho(Z) - \rho(z)\right) dz, \qquad (1)$$

where ρ is potential density, and *SI* is expressed in kg m^{-2}.

The *SI* has been calculated for all the available temperature-salinity profiles measured with the CTDs and the Argo floats. Our reference level Z is 1,500 m. When $SI = 0$, at least the upper 1,500 m of the water column is mixed. Figure 4a shows the spatial distribution of the *SI*s calculated for the region, and Figure 4b is a composite time series of those values. During January 2013, stratification regularly decreased. Vertical mixing reached 1,500 m (black dots) at the beginning of February. This deep mixed layer is observed continuously at one point or another until early March. Then, a restratification equivalent to 5 kg m^{-2} appears during a period of low heat loss (Figure 3). On March 14, low *SI* values are again observed, corresponding to a new mixing event induced by an intense wind associated with strong heat loss (Figures 2 and 3). Deep mixing is classically centered in the Gulf of Lion around 42°N, 5°E, while mixing is on average shallower in the Ligurian Sea. Highly stratified waters encircle the convection zone (red and gray squares in Figure 4a) along the general circulation pattern sketched in Figure 1.

CONVECTION: VERTICAL AND HORIZONTAL PROCESSES

To compare the impact of surface fluxes and horizontal advection on convective processes, we used the SYMPHONIE model to carry out one-dimensional simulations (without horizontal advection) of the water column at the LION mooring (Marsaleix et al., 2012). These simulations were initialized on December 6, 2012, with measurements from the deep-water mooring and a glider (which was close to mooring at this date) for intermediate and surface waters. The simulations were forced at the surface by buoyancy surface fluxes calculated with three-hourly ECMWF operational forecasts. To account for uncertainties in the turbulent heat fluxes, we used two bulk parameterizations, COARE and MOON (Moon et al., 2007), which provide the lowest and the strongest fluxes, respectively (Figure 5a).

Figure 5 compares the temperature profiles calculated with the COARE and MOON simulations with the LION mooring measurements. Simulations start with a stratified profile, then successive strong wind events with strong buoyancy losses mixing the water column are observed and simulated. Ocean convection begins earlier in the simulations than in the mooring data, particularly with MOON. Convection simulated with MOON reaches 1,500 m in January, that is, 20 days before it was detected by observations. Moreover, in February, both simulations present unrealistically low temperatures. These simulations suggest that horizontal advection by baroclinic instability, omitted in this one-dimensional vertical approach, is a major factor controlling mixed layer depth. Indeed, during the periods of positive buoyancy surface flux, the observations show restratification events in the upper 500 m (patches of warming) that limit the progress of convection and subsequent cooling once the water column is completely mixed. Studies with high-resolution realistic three-dimensional models are essential for understanding the complex interactions between buoyancy fluxes, horizontal advection, and convective processes (see Estournel et al., 2016, for a heat and water budget over the preconditioning and convective periods). Another conclusion is that turbulent heat fluxes uncertainties must be reduced.

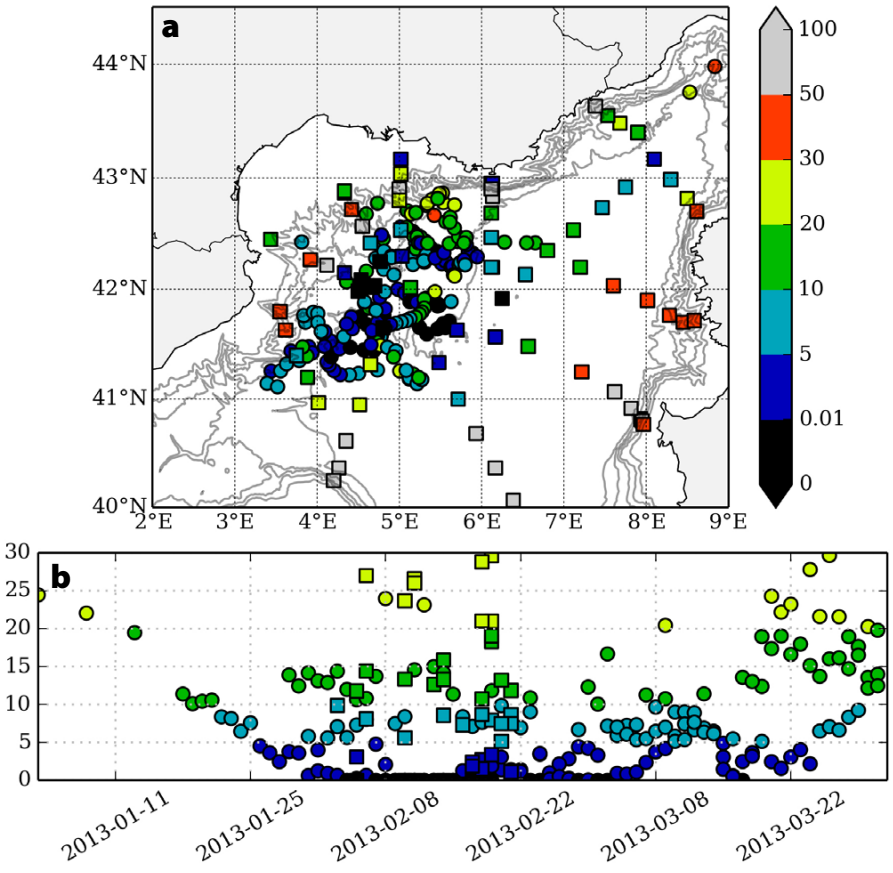

FIGURE 4. (a) Spatial distribution, and (b) time evolution from January 2012 to March 2013 of the stratification index relative to 1,500 m (kg m^{-2}) calculated from the CTD (square) and the Argo floats (circles). Note that only the stratification indices lower than 30 kg m^{-2} have been plotted in the bottom panel.

SUBMESOSCALE PROCESSES

Autonomous underwater gliders are well suited for capturing small-scale variability in convective regions. Submesoscale flows are greatly enhanced during winter as lateral density gradients intensify (Callies et al., 2015) and are responsible for increasing vertical exchanges during that season. Those processes are still poorly understood, mostly due to a lack of in situ observations.

Figure 6a shows the trajectory of a glider crossing the deep convection area in February 2013. The along-track temperature and isopycnal plots from the surface to 1,000 m depth (Figure 6c, lower panel) clearly show the mean cyclonic circulation circling the convection zone in the central part of the Gulf of Lion. By that time, the Northern Current and North Balearic Front were both characterized by a strong density gradient separating the surface Atlantic Water and underlying warm Levantine Intermediate Water from the newly formed deep water. The lateral buoyancy gradients ($b = -g\,\rho/\rho_0$, where b = buoyancy, ρ = potential density, and ρ_0 is a reference density) between the convection zone and the rim current were very intense, reaching 1–2 10^{-7} s^{-2} (see Figure 6c, upper panel). On the other hand, the vertical stratification ($N^2 = db/dz$) characterizing the static stability of the water column is drawn to almost zero in the central part of the Gulf of Lion as a result of vertical mixing.

Regarding the stability of these density fronts, potential vorticity is a key parameter that can be approximated as the difference between the vertical stratification term $A = N^2 f^2$ (where f is the Coriolis parameter) and the square of the along-track buoyancy gradients $B = (db/dx)^2$ (Thomas et al., 2013). A negative potential vorticity is a necessary condition for symmetric instability. For the sake of clarity, as well as to avoid numerous technical details, we have neglected here the vorticity of currents much smaller than f for geostrophic flows. The glider sampled the Northern Current front twice within four days (see Figure 6a, blue and

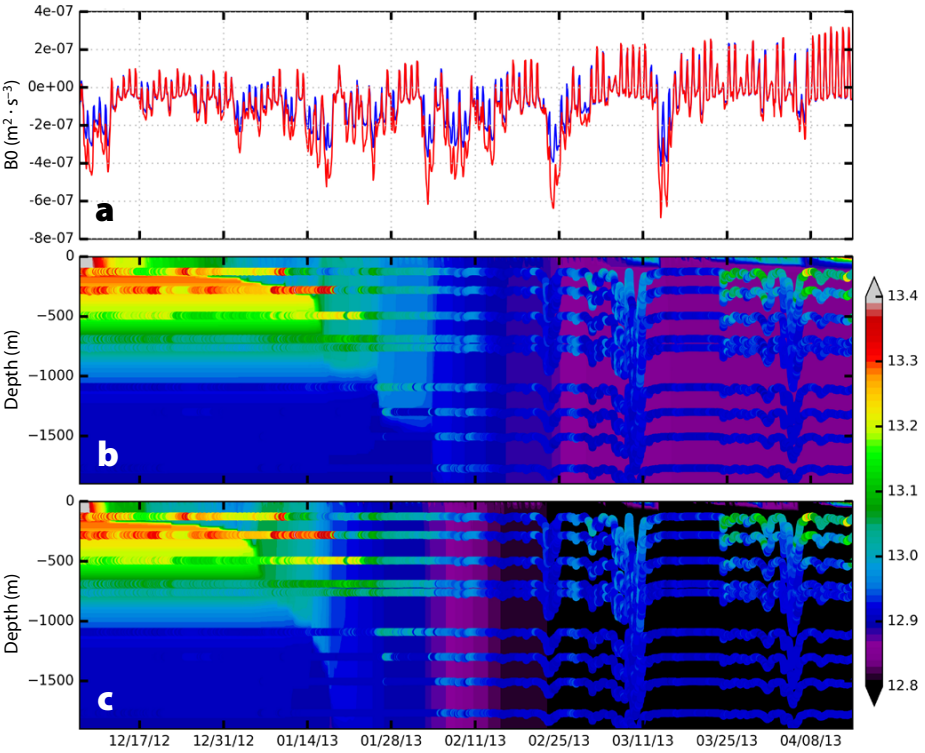

FIGURE 5. (a) Time series of the surface buoyancy flux (m^2 s^{-3}) for COARE (blue) and MOON (red) simulations. (b) and (c) Hovmöller diagrams of temperature simulated at the LION mooring with a 1DV model for (b) COARE and (c) MOON. Temperature measured at the LION mooring is superimposed with open circles.

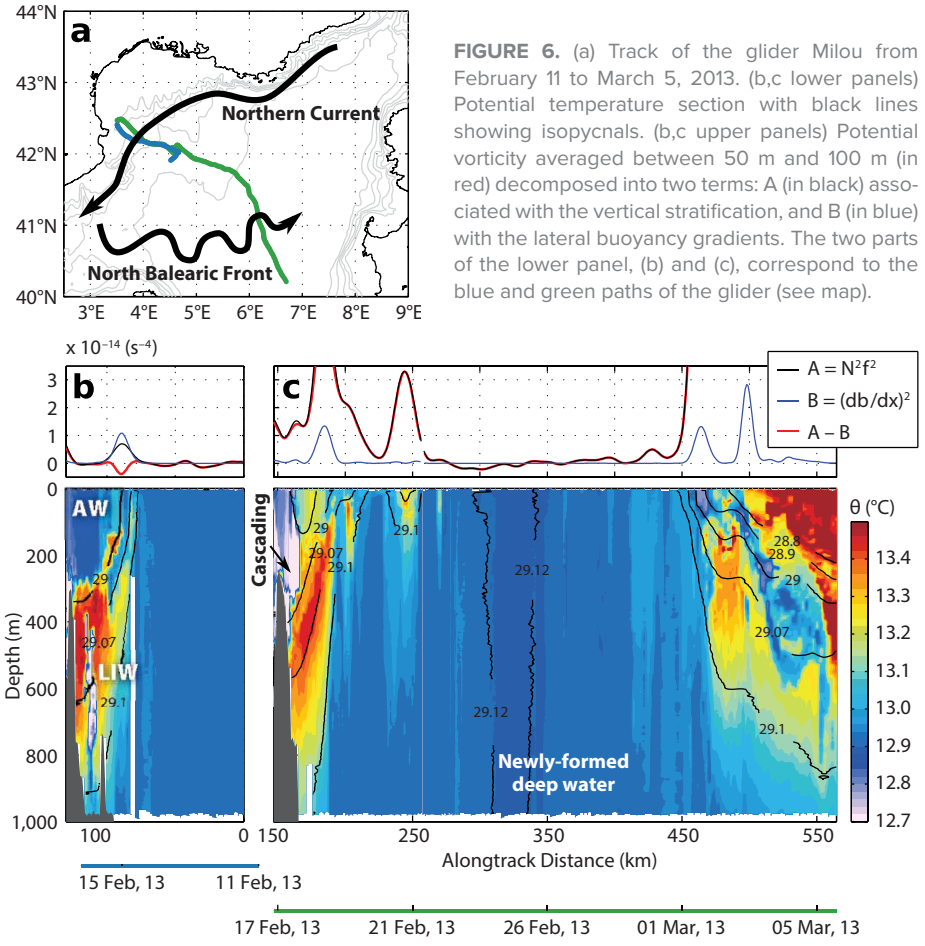

FIGURE 6. (a) Track of the glider Milou from February 11 to March 5, 2013. (b,c lower panels) Potential temperature section with black lines showing isopycnals. (b,c upper panels) Potential vorticity averaged between 50 m and 100 m (in red) decomposed into two terms: A (in black) associated with the vertical stratification, and B (in blue) with the lateral buoyancy gradients. The two parts of the lower panel, (b) and (c), correspond to the blue and green paths of the glider (see map).

green sections on the glider track), revealing its rapid evolution. On February 15 (Figure 6b), the temperature data show interleaving of warm and cold waters at the submesoscale, suggesting the presence of important vertical exchanges, while four days later (Figure 6c), the front was restored to a stable situation. The negative potential vorticity confirms that the front area was symmetrically unstable during the first crossing. Symmetric instability, known to result in triggering slanted motions connecting the surface waters to the deeper levels below the stratified front, is then responsible of the interleaving of cold and warm waters recorded by the glider. Our observations suggest that this process, recently found in the Gulf Stream (Thomas et al., 2013), could also play a crucial role in the ventilation of high- and mid-latitude deep convection zones. Of course, symmetric instability acts in concert with other sources of vertical velocities in the ocean such as static instability or frontogenesis (Giordani et al., 2006). Finally, the section crossing the Balearic Front (located at right in Figure 6c) also revealed the presence of cold waters down to about 600 m. This further reinforces the idea that vertical velocities are important at the edge of the deep convection area and are crucial for ventilating the deep ocean.

It is also noteworthy that, while exploring the western slope of the Gulf of Lion around Lacaze-Duthiers Canyon located at the northwest extremity of the track, the glider recorded a moderate cascading of shelf waters (see "cascading" indication in Figure 6c) characterized between 0 m and 650 m depth by colder (12.5°C) and fresher (38.2) waters compared to offshore waters.

COMPLEMENTARITY OF THE DATA SET: THE EXAMPLE OF AN INTENSE OBSERVATION PERIOD (IOP28 – MARCH 13–15, 2013)

A strong wind event occurred from March 13 to 15, 2013, after a week of calm weather. Figure 7c shows the 10 m winds from the SOP-dedicated AROME weather prediction system at 2.5 km resolution (AROME-WMED; Fourrié et al., 2015) on March 14 at 12:00 UTC and the 10 m winds measured at the Lion buoy (Figure 7d, top panel). They both show Mistral/Tramontane northwest winds reaching 30 m s^{-1} in the western Gulf of Lion. The aircraft flew close to the buoy

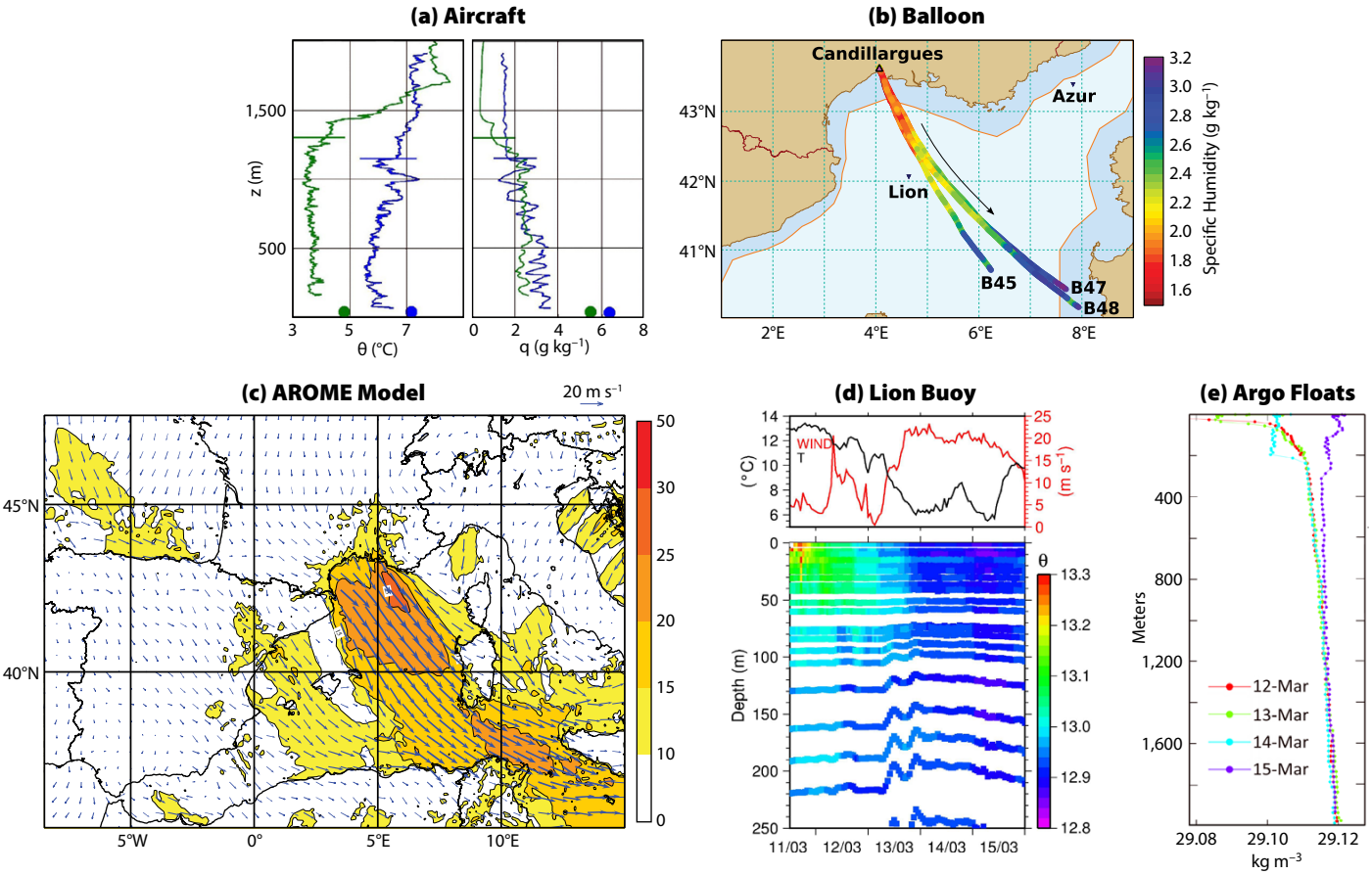

FIGURE 7. Illustrations of IOP28 (March 13–15, 2013) data. (a) Profiles of potential temperature and water vapor mixing ratio measured by the aircraft on March 14 (blue lines) and March 15 (green lines). The horizontal bars mark the top of the atmospheric boundary layer. The surface values measured at the Lion buoy during the flights are indicated on the bottom of each diagram. (b) Air specific humidity (g kg^{-1}) recorded by three balloons flying between 600 m and 900 m altitude on March 14 and 15. Rapid variations in humidity result from rapid vertical excursions of the balloons (e.g., at the end of flight 48). The orange polygon shows the authorized flight domain. (c) Wind at 10 m from AROME-WMED model on March 14 at 00:00 UTC. (d, top panel) Air temperature in black and wind in red at the Lion buoy. (d, bottom panel) Water temperature beneath the buoy. (e) Potential density recorded by Argo float 6901471 between March 12 and 15. The low values of surface density (~29.04) on March 12 are not shown for figure clarity.

on March 14 and 15 and recorded wind speeds of 20 m s^{-1} near the surface, and up to 30 m s^{-1} in the upper half of the ABL near 1,000 m (not shown). The cooling associated with the strong northwesterly winds led to a decrease of 7°C in air temperature in 48 hours at the buoy. Air and sea surface temperatures, which were both close to 13°C before the event, differed by 7°C on March 15. The air temperature drop recorded by the aircraft on March 14 and 15 (Figure 7a) was similar to that observed at the buoy during the same interval. Figure 7b presents the specific humidity recorded by three pressurized balloons drifting between 600 m and 900 m above sea level on March 14 and 15. The regular increase in humidity along the path of the air mass over the sea reflects evaporation at the air-sea interface, which fills the ABL with water vapor that is then transported with the northwesterly winds. The quite similar values measured by the three balloons indicate a rather well-mixed ABL. A large moisture difference was observed between the surface (buoy) and the ABL (see Figure 7a where the surface values have been reported) of the order of 3 g kg^{-1}, confirming significant evaporation.

Such conditions destroyed the ocean stratification present in the upper 200–300 m during the previous week, as shown by the decrease in temperature beneath the Lion buoy (Figure 7d, lower panel) and the increase in density between March 13 and 15 (Figure 7e). The surface potential density increased from 29.04 to 29.12. A new 200 m thick mixed layer is visible on the March 14 Argo profile, and on March 15, the density profile became clearly unstable. Thanks to the quality and quantity of data collected during this event, it will be possible to calculate heat and water budgets for the atmospheric and oceanic mixed layers, and to address scientific questions linked to the impact of atmospheric forcing intermittencies on convection zone restratification.

CONCLUSION

During HyMeX-SOP2 in the northwestern Mediterranean, a large set of meteorological and oceanographic observations were collected, from the regional scale to the submesoscale, and from the seasonal scale to the hourly scale.

The first results presented here indicate the importance of exchanges between the mixed patch and its stratified periphery. The cooling of the water column in the mixed patch is disrupted by intrusions of warmer water. As a result, dense water production was then lower than predicted by a one-dimensional modeling approach. Otherwise, gliders reveal the presence of strong vertical velocities related to symmetric instability developing at the edge of the convection zone. These submesoscale processes contribute to ventilation of the convection zone. Finally, the combination of atmospheric and oceanographic observations illustrates the fast response times of each medium, for example, the destruction within hours of the ocean stratification or the increases in temperature and humidity in the continental air mass over the sea.

Thanks to SOP2 observations, a fantastic benchmark is now available for modeling studies and for the year 2013. Together with the ongoing and long-term observational efforts carried out in the framework of MOOSE since 2010, we anticipate interannual variability issues could soon be addressed with fine-tuned models.

REFERENCES

Andreas, E.L., P.O.G. Persson, and J.E. Hare. 2008. A bulk turbulent air-sea flux algorithm for high-wind, spray conditions. *Journal of Physical Oceanography* 38:1,581–1,596, https://doi.org/10.1175/2007JPO3813.1.

Belamari, S., and A. Pirani. 2007. Validation of the optimal heat and momentum fluxes using the ORCA-LIM global ocean-ice model. *MERSEA IP Deliverable*, D.4.1.3, 88 pp.

Bignami, F., S. Marullo, R. Santoleri, and M.E. Schinao. 1995. Longwave radiation budget in the Mediterranean Sea. *Journal of Geophysical Research* 100(C2):2,501–2,514, https://doi.org/10.1029/94JC02496.

Bosse, A., P. Testor, L. Houpert, P. Damien, L. Prieur, D. Hayes, V. Taillandier, X. Durrieu de Madron, F. D'Ortenzio, L. Coppola, and others. 2016. Scales and dynamics of submesoscale coherent vortices formed by deep convection in the northwestern Mediterranean Sea. *Journal of Geophysical Research* 121, https://doi.org/10.1002/2016JC012144.

Bourras, D., A. Weill, G. Caniaux, L. Eymard, B. Bourlès, S. Letourneur, D. Legain, E. Key, F. Baudin, B. Piguet, and others. 2009. Turbulent air-sea fluxes in the Gulf of Guinea during the AMMA experiment. *Journal of Geophysical Research* 114, C04014, https://doi.org/10.1029/2008JC004951.

Callies, J., R. Ferrari, J.M. Klymak, and J. Gula. 2015. Seasonality in submesoscale turbulence. *Nature Communications* 6, 6862, https://doi.org/10.1038/ncomms7862.

Canut, G., M. Lothon, F. Saïd, and F. Lohou. 2010. Observation of entrainment at the interface between monsoon flow and the Saharan Air Layer. *Quarterly Journal of the Royal Meteorological Society* 136:34–46, https://doi.org/10.1002/qj.471.

Doerenbecher, A., C. Basdevant, P. Drobinski, P. Durand, C. Fesquet, F. Bernard, P. Cocquerez, N. Verdier, and A. Vargas. 2016. Low atmosphere drifting balloons: Platforms for environment monitoring and forecast improvement. *Bulletin of the American Meteorological Society* 97:1,583–1,599, https://doi.org/10.1175/BAMS-D-14-00182.1.

Drobinski, P., V. Ducrocq, P. Alpert, E. Anagnostou, K. Béranger, M. Borga, I. Braud, A. Chanzy, S. Davolio, G. Delrieu, and others. 2014. HyMeX: A 10-year multidisciplinary program on the Mediterranean water cycle. *Bulletin of the American Meteorological Society* 95:1,063–1,082, https://doi.org/10.1175/BAMS-D-12-00242.1.

Ducrocq, V., I. Braud, S. Davolio, R. Ferretti, C. Flamant, A. Jansa, N. Kalthoff, E. Richard, I. Taupier-Letage, P.A. Ayral, and others. 2014. HyMeX-SOP1: The field campaign dedicated to heavy precipitation and flash-flooding in the Northwestern Mediterranean. *Bulletin of the American Meteorological Society* 95:1,083–1,100, https://doi.org/10.1175/BAMS-D-12-00244.1.

Estournel, C., P. Testor, P. Damien, F. D'Ortenzio, P. Marsaleix, P. Conan, F. Kessouri, X. Durrieu de Madron, L. Coppola, J.M. Lellouche, and others. 2016. High resolution modeling of dense water formation in the north-western Mediterranean during winter 2012–2013: Processes and budget. *Journal of Geophysical Research* 121(7):5,367–5,392, https://doi.org/10.1002/2016JC011935.

Fairall, C.W, E.F. Bradley, J.E. Hare, A.A. Grachev, and J.B. Edson. 2003. Bulk parameterization of air-sea fluxes: Updates and verification for the COARE algorithm. *Journal of Climate* 16:571–591, https://doi.org/10.1175/1520-0442(2003)016<0571:BPOASF>2.0.CO;2.

Fourrié, N., E. Bresson, M. Nuret, C. Jany, P. Brousseau, A. Doerenbecher, M. Kreitz, O. Nuissier, E. Sevault, H. Bénichou, and others. 2015. AROME-WMED, a real-time mesoscale model designed for the HyMeX special observation periods. *Geoscientific Model Development* 8:1,919–1,941, https://doi.org/10.5194/gmd-8-1919-2015.

Giordani, H., L. Prieur, and G. Caniaux. 2006. Advanced insights into sources of vertical velocity in the ocean. *Ocean Dynamics* 56(5–6):513–524, https://doi.org/10.1007/s10236-005-0050-1.

Hauser, D., H. Branger, S. Bouffies-Cloché, S. Despiau, W. Drennan, H. Dupuis, P. Durand, X. Durrieu de Madron, C. Estournel, L. Eymard, and others. 2003. The FETCH experiment: An overview. *Journal of Geophysical Research* 108, 8053, https://doi.org/10.1029/2001JC001202.

Herrmann, M., S. Somot, F. Sevault, C. Estournel, and M. Déqué. 2008. Modeling the deep convection in the northwestern Mediterranean Sea using an eddy-permitting and an eddy-resolving model: Case study of winter 1986–1987. *Journal of Geophysical Research* 113, C04011, https://doi.org/10.1029/2006JC003991.

Houpert, L., X. Durrieu de Madron, P. Testor, A. Bosse, F. D'Ortenzio, M.N. Bouin, D. Dausse, H. Le Goff, S. Kunesch, M. Labaste, and others.

2016. Observations of open-ocean deep convection in the northwestern Mediterranean Sea: Seasonal and interannual variability of mixing and deep water masses for the 2007–2013 period. *Journal of Geophysical Research* 121, https://doi.org/10.1002/2016JC011857.

Marsaleix, P., F. Auclair, T. Duhaut, C. Estournel, C. Nguyen, and C. Ulses. 2012. Alternatives to the Robert-Asselin filter. *Ocean Modelling* 41:53–66, https://doi.org/10.1016/j.ocemod.2011.11.002.

Marshall, J., and F. Schott. 1999. Open-ocean convection: Observations, theory, and models. *Reviews of Geophysics* 37(1):1–64, https://doi.org/10.1029/98RG02739.

MEDOC Group. 1970. Observations of formation of deep-water in the Mediterranean Sea, 1969. *Nature* 227:1,037–1,040, https://doi.org/10.1038/2271037a0.

Mertens, C., and F. Schott. 1998. Interannual variability of deep-water formation in the northwestern Mediterranean. *Journal of Physical Oceanography* 28:1,410–1,424, https://doi.org/10.1175/1520-0485(1998)028<1410:IVODWF>2.0.CO;2.

Moon, I.J., I. Ginis, T. Hara, and B. Thomas. 2007. A physics-based parameterization of air-sea momentum flux at high wind speeds and its impact on hurricane intensity predictions. *Monthly Weather Review* 135:2,869–2,878, https://doi.org/10.1175/MWR3432.1.

Oost, W.A., G.J. Komen, C.M.J. Jacobs, and C. Van Oort. 2002. New evidence for a relation between wind stress and wave age from measurements during ASGAMAGE. *Boundary-Layer Meteorology* 103:409–438, https://doi.org/10.1023/A:1014913624535.

Send, U., J. Font, and C. Mertens. 1996. Recent observation indicates convection's role in deep water circulation. *Eos, Transactions American Geophysical Union* 77(7):61–65, https://doi.org/10.1029/96EO00040.

Somot, S., L. Houpert, F. Sevault, P.Testor, A. Bosse, I. Taupier-Letage, M.N. Bouin, R. Waldman, C. Cassou, E. Sanchez-Gomez, and others. 2016. Characterizing, modelling and understanding the climate variability of the deep water formation in the north-western Mediterranean Sea. *Climate Dynamics*, https://doi.org/10.1007/s00382-016-3295-0.

Taylor, P.K., and M.J. Yelland. 2001. The dependence of sea surface roughness on the height and steepness of the waves. *Journal of Physical Oceanography* 31:572–590, https://doi.org/10.1175/1520-0485(2001)031<0572:TDOSSR>2.0.CO;2.

Testor, P., and J.C. Gascard. 2006. Post-convection spreading phase in the northwestern Mediterranean Sea. *Deep Sea Research Part I* 53:869–893, https://doi.org/10.1016/j.dsr.2006.02.004.

Thomas, L.N., J.R. Taylor, R. Ferrari, and T.M. Joyce. 2013. Symmetric instability in the Gulf Stream. *Deep Sea Research Part II* 91:96–110, https://doi.org/10.1016/j.dsr2.2013.02.025.

Visbeck, M., J. Marshall, and H. Jones. 1996. Dynamics of isolated convective regions in the ocean. *Journal of Physical Oceanography* 26:1,721–1,734, https://doi.org/10.1175/1520-0485(1996)026<1721:DOICRI>2.0.CO;2.

Waldman, R., S. Somot, M. Herrmann, P. Testor, C. Estournel, F. Sevault, L. Prieur, L. Mortier, L. Coppola, V. Taillandier, and others. 2016. Estimating dense water volume and its evolution for the year 2012–2013 in the North-western Mediterranean Sea: An Observing System Simulation Experiment approach. *Journal of Geophysical Research* 121:6,696–6,716, https://doi.org/10.1002/2016JC011694.

ACKNOWLEDGMENTS

Many people participated in SOP2: scientists, technicians, crews, and people in charge of the organization. All deserve our grateful thanks. HyMeX-SOP2 was supported by CNRS, Météo-France, IFREMER, and CNES through the international metaprogramme MISTRALS dedicated to the understanding of Mediterranean basin environmental processes (http://www.mistrals-home.org); by the ANR-12-BS06-0003 ASICS-MED; and by the EU-FP7 PERSEUS (GA 287600), JERICO (GA 262584), and GROOM (GA 284321). Five Argo floats were provided by LEFE/GMMC. Important data sets were provided by the French MOOSE (ALLENVI-INSU) and MERMEX-DEWEX programs. Large amounts of data are available in the HyMeX database for noncommercial research. Other data, such as Argo and glider profiles, are archived in the CORIOLIS data center for operational oceanography.

AUTHORS

Claude Estournel (claude.estournel@aero.obs-mip.fr) is Directrice de Recherche, Université de Toulouse; CNRS, Laboratoire d'Aérologie, Toulouse, France. **Pierre Testor** is Chargé de Recherche, CNRS; IRD; UPMC Université de Paris 06; MNHN, LOCEAN, Paris, France. **Isabelle Taupier-Letage** is Chargée de Recherche, Aix Marseille Université; CNRS; Université de Toulon; IRD, MIO, Marseille, France. **Marie-Noelle Bouin** is Researcher, CNRM/CMM, Météo-France, Brest, France, and CNRM, UMR3589, Météo-France and CNRS, Toulouse, France. **Laurent Coppola** is Physicien, Sorbonne Universités; UPMC Université de Paris 06; CNRS, LOV, Villefranche-sur-Mer, France. **Pierre Durand** is Directeur de Recherche, Université de Toulouse; CNRS, Laboratoire d'Aérologie, Toulouse, France. **Pascal Conan** is Maître de Conférences, Sorbonne Universités; UPMC Université de Paris; CNRS, LOMIC, Banyuls-sur-Mer, France. **Anthony Bosse** is Postdoctoral Researcher, CNRS; IRD; UPMC Université de Paris; MNHN, LOCEAN, Paris, France. **Pierre-Etienne Brilouet** is PhD, Université de Toulouse; CNRS, Laboratoire d'Aérologie, Toulouse, France and CNRM, UMR3589, Météo-France and CNRS, Toulouse, France. **Laurent Beguery** was Ingénieur, INSU Division Technique, La Seyne sur Mer, France, and is currently Ingénieur, ACSA, Meyreuil, France. **Sophie Belamari** is Researcher, CNRM, UMR3589, Météo-France and CNRS, Toulouse, France. **Karine Béranger** is Maître de Conférences, CNRS; ENS; Ecole Polytechnique; UPMC, LMD, Palaiseau, France. **Jonathan Beuvier** is Researcher, MERCATOR-OCEAN, Ramonville-Saint-Agnés, France. **Denis Bourras** was Researcher, Université Versailles Saint-Quentin-en-Yvelines; Sorbonne Universités, UPMC Université de Paris 06; CNRS, LATMOS-IPSL, Guyancourt, France, and is currently at Aix Marseille Université; CNRS; Université de Toulon; IRD, MIO, Marseille, France. **Guylaine Canut** is Researcher, CNRM, UMR3589, Météo-France and CNRS, Toulouse, France. **Alexis Doerenbecher** is Researcher, CNRM, UMR3589, Météo-France and CNRS, Toulouse, France. **Xavier Durrieu de Madron** is Directeur de Recherche, Université de Perpignan; CNRS, Perpignan, France. **Fabrizio D'Ortenzio** is Chargé de Recherche, Sorbonne Universités; UPMC Université de Paris 06; CNRS, LOV, Villefranche-sur-Mer, France. **Philippe Drobinski** is Directeur de Recherche, CNRS; ENS; École Polytechnique; UPMC, LMD, Palaiseau, France. **Véronique Ducrocq**, **Nadia Fourrié**, and **Hervé Giordani** are Researchers, CNRM, UMR3589, Météo-France and CNRS, Toulouse, France. **Loïc Houpert** is Postdoctoral Scientist, Scottish Association for Marine Science, Scottish Marine Institute, Oban, Argyll, United Kingdom. **Laurent Labatut** is Ingénieur, **Cindy Lebeaupin Brossier** is Chargée de Recherche, and **Mathieu Nuret** is Researcher, CNRM, UMR3589, Météo-France and CNRS, Toulouse, France. **Louis Prieur** is Directeur de Recherche, Sorbonne Universités; UPMC Univ Paris 06; CNRS, LOV, Villefranche-sur-Mer, France. **Odile Roussot** is Ingénieur, CNRM, UMR3589, Météo-France and CNRS, Toulouse, France. **Leo Seyfried** is PhD, Université de Toulouse; CNRS, Laboratoire d'Aérologie, Toulouse, France. **Samuel Somot** is Researcher, CNRM, UMR3589, Météo-France and CNRS, Toulouse, France.

ARTICLE CITATION

Estournel, C., P. Testor, I. Taupier-Letage, M.-N. Bouin, L. Coppola, P. Durand, P. Conan, A. Bosse, P.-E. Brilouet, L. Beguery, S. Belamari, K. Béranger, J. Beuvier, D. Bourras, G. Canut, A. Doerenbecher, X. Durrieu de Madron, F. D'Ortenzio, P. Drobinski, V. Ducrocq, N. Fourrié, H. Giordani, L. Houpert, L. Labatut, C.L. Brossier, M. Nuret, L. Prieur, O. Roussot, L. Seyfried, and S. Somot. 2016. HyMeX-SOP2: The field campaign dedicated to dense water formation in the northwestern Mediterranean. *Oceanography* 29(4):196–206, https://doi.org/10.5670/oceanog.2016.94.